

Cubic autocatalytic reaction–diffusion equations: semi-analytical solutions

BY T. R. MARCHANT

*School of Mathematics and Applied Statistics, The University of Wollongong,
Wollongong, 2522 NSW, Australia (tim_marchant@uow.edu.au)*

Received 3 January 2001; revised 16 July 2001; accepted 30 July 2001

The Gray–Scott model of cubic-autocatalysis with linear decay is coupled with diffusion and considered in a one-dimensional reactor (a reaction–diffusion cell). The boundaries of the reactor are permeable, so diffusion occurs from external reservoirs which contain fixed concentrations of the reactant and catalyst.

The Galerkin method is used to approximate the spatial structure of the reactant and autocatalyst concentrations in the reactor. Ordinary differential equations are then obtained as an approximation to the governing partial differential equations. The ordinary differential equations are then analysed to obtain semi-analytical results for the reaction–diffusion cell.

Steady-state concentration profiles and bifurcation diagrams are obtained both explicitly, for the one-term method, and as the solution to a pair of transcendental equations, for the two-term method. Singularity theory is used to determine the regions of parameter space in which the four main types of bifurcation diagram occur. Also, in the semi-analytical model, a fifth bifurcation diagram occurs in an extremely small parameter region; its size being $O(10^{-10})$.

The region of parameter space, in which Hopf bifurcations can occur, is found by a local stability analysis of the semi-analytical model. An example of a stable limit-cycle is also considered in detail. The usefulness and accuracy of the semi-analytical results are confirmed by comparison with numerical solutions of the governing partial differential equations.

Keywords: Author: please supply up to six keywords/phrases!

1. Introduction

There is a great deal of interest in chemical reactions which exhibit oscillatory solutions. These oscillations occur due to feedback in the system; either chemical feedback (such as autocatalysis) or temperature feedback due to a non-isothermal reaction. Two well-studied examples of reactions exhibiting oscillatory solutions are the isothermal Belousov–Zhabotinsky reaction and the Sal’nikov thermokinetic oscillator. The continuous-flow well-stirred tank reactor (the CSTR) has proved convenient for both experimental and theoretical studies as open systems allow the existence of steady-states and sustained oscillations. Also, the governing system of ordinary differential equations can be readily analysed using the standard techniques of bifurcation theory, with analytical results often possible.

The Gray–Scott scheme, which represents cubic-autocatalysis with linear catalyst decay, has been much considered, because of its multiple steady-state responses and oscillatory solutions. See Gray (1988) and Gray & Scott (1990) for reviews and descriptions of much of this work. The scheme is



where the concentrations of the reactant and autocatalyst are a and b , respectively. The parameters β and γ are rate constants. The catalyst is not stable, but undergoes a simple linear decay to a product C . This allows a much wider variety of behaviour in the system, than does the cubic reaction alone.

Gray & Scott (1983) and Gray & Scott (1984) analyse the system (1.1) in the CSTR. They found that three types of steady-state bifurcation diagrams occur, termed the unique, mushroom and isola patterns. Moreover, a local stability analysis was performed with the parameter region found in which Hopf bifurcations occur. The ordinary differential equations were also solved numerically to illustrate the evolution of the system in various scenarios, such as stable and unstable limit-cycles and oscillatory decay to a stable steady state. Kay *et al.* (1987) showed that the addition of an uncatalysed conversion step ($A \rightarrow B$) increased the number of different bifurcation diagrams to five, the new ones being a breaking-wave pattern, with and without an isola. The breaking-wave plus isola pattern was found to occur in an extremely small parameter region and is associated with the winged-cusp singularity.

Scott (1987) and Kay & Scott (1988) considered the reaction scheme (1.1) when the mixture is not well-stirred. In this case the system is described by coupled partial differential equations which include the effects of both reaction and diffusion. In contrast to the CSTR model, results must be obtained numerically for the diffusive model. Four of the five steady-state bifurcation diagrams discussed above were identified. The breaking-wave plus isola pattern was also assumed to occur, but in a parameter region too small to be found numerically. The parameter choices, for which Hopf bifurcations occur, were also found. This involved calculating the eigenvalues of the Jacobian of the system of discretized partial differential equations.

Microwave heating is described by a reaction–diffusion equation, which governs the absorption and diffusion of heat in the material, plus an ordinary differential equation, which describes the propagation and decay of the time-harmonic microwave radiation. The two equations are coupled via the temperature dependence of the material properties. The steady-state temperature response is a S-shaped curve, hence thermal runaway occurs at a particular power level, when the solution jumps from the cool to the hot branch. Marchant & Liu (1998) and Liu & Marchant (1999) considered the steady-state microwave heating of finite one- and two-dimensional slabs. The temperature dependency of the material properties was modelled by an Arrhenius-type law. As this law is not analytically amenable, it was approximated by a rational-cubic function. This allowed semi-analytical solutions to be found for the temperature and the electric-field amplitude, using the Galerkin method. Moreover, an excellent comparison with numerical solutions of the governing equations was obtained.

In this paper the cubic-autocatalytic scheme with linear decay (1.1) is examined in a simple one-dimensional reaction–diffusion cell. This system of equations has been considered by Kay & Scott (1988) numerically; here the Galerkin method will be used to develop semi-analytical solutions. In §2 the governing equations are presented

and the Galerkin method is used to obtain the ordinary differential equations which represent the semi-analytical model. In § 3 both steady-state concentration profiles and bifurcation patterns are presented and described in detail. In § 4 singularity theory is used to calculate the hysteresis and isola bifurcation points. The loci of bifurcation points are plotted and the regions of parameter space are identified in which the four main bifurcation patterns occur. The parameter region in which the fifth bifurcation diagram occurs, in the semi-analytical model, is also found. In § 5 a local stability analysis of the semi-analytical model is performed. The double-zero eigenvalue and transversality degenerate Hopf points are found; hence the parameter region in which Hopf bifurcations occur is identified. An example of a stable limit-cycle is also considered. Comparisons are made throughout the paper between the semi-analytical results and numerical solutions of the governing partial differential equations. The appendix contains the two transcendental equations which describe the steady-state two-term semi-analytical solution.

2. The semi-analytical model

(a) The governing equations

The cubic-autocatalytic reaction with linear decay (1.1), is considered in a one-dimensional reaction–diffusion cell. The governing partial differential equations are


$$\left. \begin{aligned} a_t &= a_{xx} - \beta ab^2, & b_t &= b_{xx} + \beta ab^2 - \beta \gamma b, \\ a_x = b_x &= 0 \quad \text{at } x = 0, & a = 1, \quad b = b_0 & \quad \text{at } x = 1 \text{ and } t = 0. \end{aligned} \right\} \quad (2.1)$$

The system (2.1) is in non-dimensional form with the concentrations of the reactant and autocatalyst given by a and b , respectively. It is an open system; the reactor has a permeable boundary at $x = 1$, joined to a reservoir which contains a and b at constant concentrations. The boundary condition at $x = 0$ is a symmetry condition; an identical reservoir is located at $x = -1$. The system is characterized by three non-dimensional parameters. The ratio of the autocatalyst and reactant concentrations in the reservoir is b_0 . The parameter β is a measure of the importance of the reaction terms, compared with diffusion, while γ is a measure of the importance of autocatalyst decay, compared with the cubic-reaction. The simplest way to adjust the non-dimensional parameters experimentally is by changing the reservoir concentrations. Other possibilities for varying the non-dimensional parameters include changing the diffusivity of the system or the length of the reactor. The diffusivity could be changed by adjusting the temperature or by the addition of otherwise inactive salts. See Scott (1987) for a fuller discussion of these possibilities.

Numerical solutions of (2.1) are found using the explicit FTCS finite-difference scheme. The steady-state solutions are found by stepping forward in time until the solution is stationary. Normally the initial condition used is the steady-state solution found for the previous value of β ; hence only a moderate amount of calculation is needed to generate a complete steady-state bifurcation curve.

Spell out?

(b) The Galerkin method

In the Galerkin method, assumptions are made about the spatial structure of the concentration profiles, which allows  governing partial differential equations (2.1)

to be approximated by ordinary differential equations. The method requires that the exact concentrations be approximated by a series of orthogonal basis functions. The expansion,

$$\left. \begin{aligned} a(x, t) &= 1 + a_1(t) \cos\left(\frac{1}{2}\pi x\right) + a_2(t) \cos\left(\frac{3}{2}\pi x\right), \\ b(x, t) &= b_0 + b_1(t) \cos\left(\frac{1}{2}\pi x\right) + b_2(t) \cos\left(\frac{3}{2}\pi x\right), \end{aligned} \right\} \quad (2.2)$$

represents the two-term method used here. Expansion (2.2) satisfies the boundary conditions in (2.1), but not the governing partial differential equations. The free parameters in (2.2) are found by evaluating averaged versions of the governing equations, weighted by the basis functions. This procedure gives the ordinary differential equations,

$$\left. \begin{aligned} \frac{da_1}{dt} &= -a_1 \frac{\pi^2}{4} - \beta N_1, & \frac{db_1}{dt} &= -b_1 \frac{\pi^2}{4} + \beta N_1 - \beta \gamma \left(b_1 + \frac{4}{\pi} b_0 \right), \\ \frac{da_2}{dt} &= -a_2 \frac{9\pi^2}{4} - \beta N_2, & \frac{db_2}{dt} &= -b_2 \frac{9\pi^2}{4} + \beta N_2 - \beta \gamma \left(b_2 - \frac{4}{3\pi} b_0 \right), \end{aligned} \right\} \quad (2.3)$$

where the expressions for N_1 and N_2 are given by

$$\left. \begin{aligned} N_1 &= a_1 b_0^2 + \frac{16}{3\pi} a_1 b_0 b_1 + \frac{16}{15\pi} a_1 b_0 b_2 + \frac{3}{4} a_1 b_1^2 + \frac{1}{2} a_1 b_1 b_2 \\ &\quad + \frac{1}{2} a_1 b_2^2 + \frac{16}{15\pi} a_2 b_0 b_1 + \frac{144}{35\pi} a_2 b_0 b_2 + \frac{1}{4} a_2 b_1^2 + \frac{1}{2} a_2 b_1 b_2 \\ &\quad + \frac{4}{\pi} b_0^2 + 2b_0 b_1 + \frac{8}{3\pi} b_1^2 + \frac{16}{15\pi} b_1 b_2 + \frac{72}{35\pi} b_2^2, \\ N_2 &= \frac{16}{15\pi} a_1 b_0 b_1 + \frac{144}{35\pi} a_1 b_0 b_2 + \frac{1}{4} a_1 b_1^2 + a_1 b_1 b_2 + a_2 b_0^2 \\ &\quad + \frac{144}{35\pi} a_2 b_0 b_1 - \frac{16}{9\pi} a_2 b_0 b_2 + \frac{1}{2} a_2 b_1^2 - \frac{3}{4} a_2 b_2^2 - \frac{4}{3\pi} b_0^2 \\ &\quad + 2b_0 b_2 + \frac{8}{15\pi} b_1^2 + \frac{144}{35\pi} b_1 b_2 - \frac{8}{9\pi} b_2^2. \end{aligned} \right\} \quad (2.4)$$

The series (2.2) has been truncated after two terms. The number of terms which need to be included in the truncated series represents a trade-off between the accuracy and complexity of the semi-analytical solution. It is found that a two-term method gives sufficient accuracy without excessive expression swell. Due to its explicit nature the one-term solution (when $a_2 = b_2 = 0$) is also calculated.

3. Steady-state solutions

Manipulating the steady-state versions of (2.3) gives explicit expressions for a_1 and a_2 as

$$a_1 = -b_1 - \frac{4}{\pi^2} \beta \gamma \left(b_1 + \frac{4}{\pi} b_0 \right), \quad a_2 = -b_2 - \frac{4}{9\pi^2} \beta \gamma \left(b_2 - \frac{4}{3\pi} b_0 \right), \quad (3.1)$$

which are substituted back into (2.3) to obtain two transcendental equations, (A 1) and (A 2), for the unknowns b_1 and b_2 at the steady state. The one-term solution (where $a_2 = b_2 = 0$) can be written as a quadratic equation for β ,

$$f = \frac{\gamma m}{\pi^2} \beta^2 + n\beta + \frac{\pi^2}{8} b_1 = 0, \quad (3.2)$$

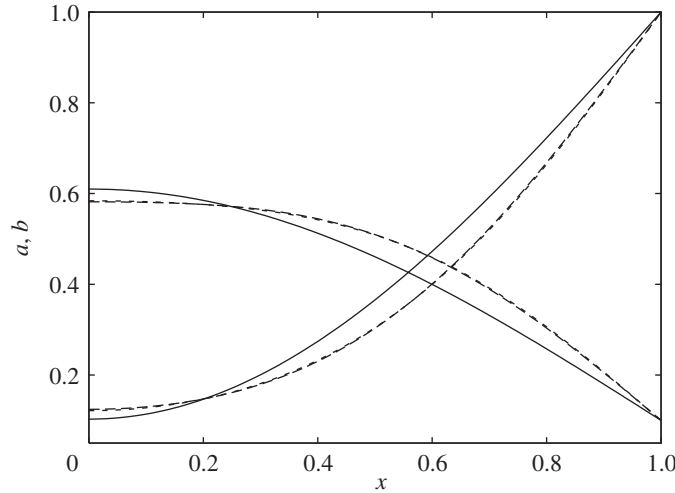


Figure 1. Steady-state reactant and autocatalyst concentration profiles. The parameters are $b_0 = 0.1$, $\gamma = 0.05$ and $\beta = 30$. Shown is the one-term (solid line) and two-term (large dashes) semi-analytical solutions and the numerical solution of (2.1) (small dashes).

where

$$m = \frac{3}{2}b_1^3 + \frac{50}{3\pi}b_0b_1^2 + \frac{128}{3\pi^2}b_1b_0^2 + 2b_1b_0^2 + \frac{8}{\pi}b_0^3,$$

$$n = \frac{3}{8}b_1^3 + \frac{8}{3\pi}b_0b_1^2 + \frac{1}{2}b_0^2b_1 - \frac{4}{3\pi}b_1^2 - b_0b_1 + \frac{2}{\pi}b_0^2 + \frac{1}{2}\gamma b_1 + \frac{2}{\pi}\gamma b_0.$$

Hence, the one-term steady-state solution can be found explicitly. For the two-term solution the transcendental equations (A 1) and (A 2) must be solved numerically, which is done using a root-finding routine from the IMSL library.

Figure 1 shows steady-state concentration profiles of the reactant and the autocatalyst. The parameters are $b_0 = 0.1$, $\gamma = 0.05$ and $\beta = 30$. Shown is one-term (solid line) and two-term (large dashes) semi-analytical solutions and the numerical solutions of (2.1) (small dashes). Catalyst production in the reactor depends on the relative importance of the cubic-reaction, compared with the linear decay. This can be determined by examining the sign of the source term in the autocatalyst equation, $\beta ab^2 - \beta \gamma b$. For this example, $\gamma < ab$, throughout the reactor, so the source term is positive. At the steady-state autocatalyst production must be balanced by the diffusive flux of autocatalyst, which is proportional to $-b_x$, from the reactor into the reservoir. As the flux is towards the boundary at $x = 1$, then the slope of the concentration profile is negative, which in turn implies that a central maximum occurs at the centre of the reactor. Similar reasoning explains the central minimum in the reactant's profile. The comparison between the two-term semi-analytical and numerical solutions is excellent, while the one-term solution is reasonably accurate.

Figure 2 shows the steady-state autocatalyst concentration profile. The parameters are $b_0 = 0.143$, $\gamma = 0.08$ and $\beta = 87$. The autocatalyst concentration profile is quite different to that in figure 1, as it has a non-central maximum. Here, the source term is positive ($\gamma < ab$) at the boundary $x = 1$. Inside the reactor, as x decreases, the product ab decreases, as the decrease in a is much greater than the increase in b . The decay rate γ is larger here than in figure 1, so the source term becomes negative

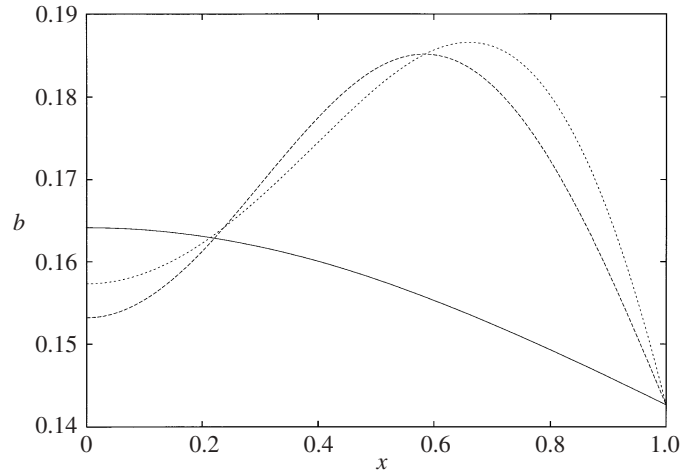


Figure 2. Steady-state autocatalyst concentration profile. The parameters are $b_0 = 0.143$, $\gamma = 0.08$ and $\beta = 87$. Shown is the one-term (solid line) and two-term (large dashes) semi-analytical solutions and the numerical solution of (2.1) (small dashes).

($\gamma > ab$) in the central region of the reactor. Near the boundary autocatalyst is being produced, hence the flux of autocatalyst into the reservoir implies that the profile has negative slope. Near the centre of the reactor autocatalyst is being consumed; hence the flux of autocatalyst is towards the centre and the slope is positive. Hence, as the profile is continuous, there must be a non-central peak in the autocatalyst profile. As the reactant profile is qualitatively similar to that in figure 1, it is not shown. It has a central minimum because the source term of the reactant equation, $-\beta ab^2$, is negative throughout the reactor. The comparison of the two-term and numerical solutions is very good, while the one-term solution is inaccurate. This is simply due to the choice of trial functions; the one-term solution is constrained to have a central maximum, while the two-term solution allows the peak to migrate away from the reactor's centre. As autocatalyst profiles with a non-central peak are associated with stable limit-cycles (see fig. 9 in Kay & Scott (1988)), it is important for the semi-analytical solution to model this feature accurately.

Figure 3 shows steady-state concentration profiles: (a) is the reactant while (b) is the autocatalyst. The parameters are $b_0 = \gamma = 0.2$ and $\beta = 108$. The linear decay of the autocatalyst dominates the cubic-reaction term, so $\gamma > ab$ throughout the reactor, and the autocatalyst profile has a central minimum. Also, as β is large, the diffusive effects are small and the autocatalyst profile is very flat near the centre of the reactor. It can be seen that the two-term and numerical solutions are very close; the one-term solution is invalid as it predicts a negative concentration at $x = 0$. As $\beta \rightarrow \infty$ a singular limit is approached, in which the diffusivity becomes vanishingly small. In this limit the profile flattens out over the whole domain, leaving a boundary layer near $x = 1$. In this case the two-term solution would also break down as additional terms are needed in the series (2.2) to model the flat concentration profile.

The bifurcation diagrams show the steady-state autocatalyst concentration at the reactor's centre, $b_0 + b_1 + b_2$, versus the bifurcation parameter β . Figure 4 shows bifurcation diagrams representing each of the four main patterns. They are (a) the unique pattern, with $\gamma = b_0 = 0.2$, (b) the breaking-wave pattern, with $\gamma = 0.05$ and

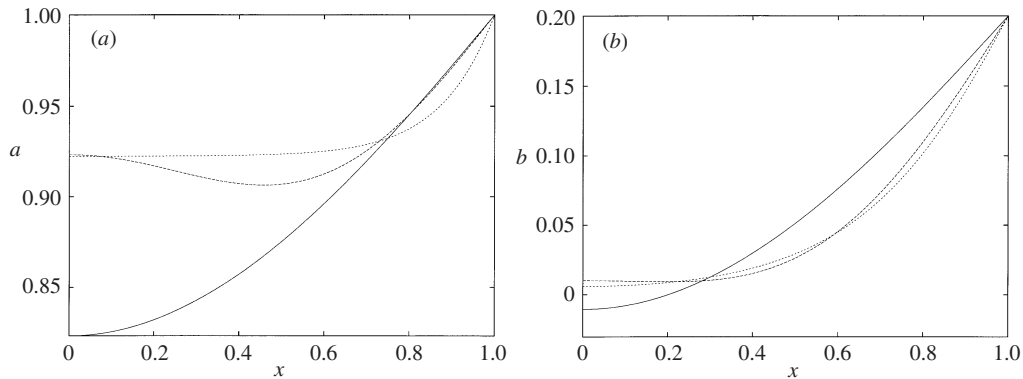


Figure 3. Steady-state concentration profiles; (a) is the reactant while (b) is the autocatalyst. The parameters are $b_0 = \gamma = 0.2$ and $\beta = 108$. Shown is the one-term (solid line) and two-term (large dashes) semi-analytical solutions and the numerical solution of (2.1) (small dashes).

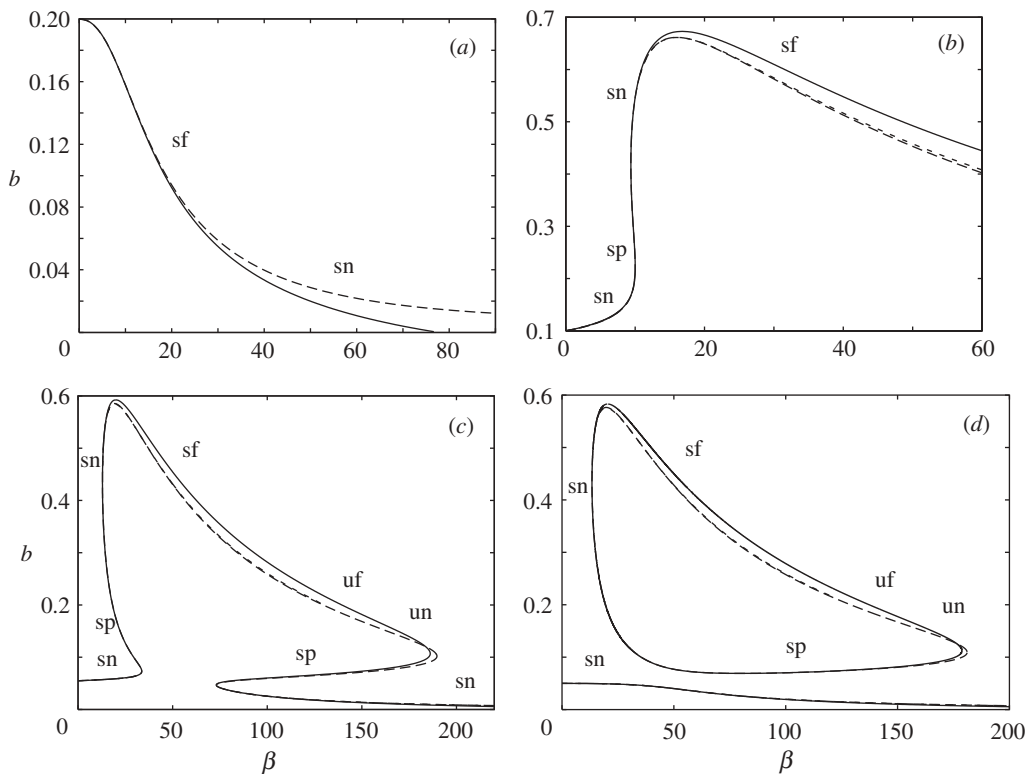


Figure 4. Steady-state bifurcation diagrams; the autocatalyst concentration, $b_0 + b_1 + b_2$ versus β . (a) is the unique pattern, with $\gamma = b_0 = 0.2$, (b) is the breaking-wave pattern with $\gamma = 0.05$ and $b_0 = 0.1$, (c) is the mushroom pattern, with $\gamma = 0.05$ and $b_0 = 0.055$, and (d) is the isola pattern, with $\gamma = b_0 = 0.05$. Shown is the one-term (solid lines) and two-term (large dashes) semi-analytical solutions plus the numerical solution of (2.1) (small dashes).

$b_0 = 0.1$, (c) the mushroom pattern, with $\gamma = 0.05$ and $b_0 = 0.055$, and (d) the isola pattern, with $\gamma = b_0 = 0.05$. Shown is the one-term (solid lines) and two-term (large dashes) semi-analytical solutions plus the numerical solution of (2.1) (small dashes). The labels on the figures indicate the stability of that portion of the steady-state curve, as found from the local stability analysis of the semi-analytical solution in § 5. The types of local stability are stable node (sn), stable focus (sf), saddle point (sp), unstable focus (uf) and unstable node (un). Also, there is a small region of steady-state solution which is a stable focus, and is unlabelled. It occurs for both the mushroom and isola patterns on the low conversion branch, at large values of β .

Three of these bifurcation diagrams have a region where three steady-state solutions exist. These three bifurcation patterns all have ignition and/or washout points which respond to a jump between steady-states having vastly different rates of conversion of the reactant a to autocatalyst b . The breaking-wave pattern has an ignition and a washout point, the isola pattern has two washout points while the mushroom pattern has two ignition and two washout points. In general the comparison between the two-term semi-analytical and the numerical solutions is excellent. Moreover, the one-term solution is generally accurate, except when β is large or on the upper branch of the mushroom or isola curves, when a non-central peak develops in the autocatalyst concentration profile. As the one-term solutions are found explicitly from the quadratic equation (3.2), its accuracy is particularly notable. Only the stable portions of the numerical curve are presented. In particular, it can be seen on the upper branch of the isola and mushroom diagrams that the numerical solution loses stability as β increases. These are points of Hopf bifurcation, which lead to limit-cycles. For these examples the limit-cycles are unstable and the solution evolves to a stable steady-state on the lower solution branch.

4. Singularity theory

Singularity theory allows a complete description of all qualitatively distinct behaviour, which occurs in a particular system of ordinary differential equations. This is done by calculating the degenerate singular points, the most degenerate point being the organizing centre of the system. An excellent text on the application of singularity theory to bifurcation problems is Golubitsky & Schaeffer (1985). The application of singularity theory to chemical reactions is described in Balakotaiah & Luss (1983). They give conditions for the hysteresis and isola bifurcation curves and apply the theory to examples involving first-order, non-isothermal reactions in a CSTR.

Singularity theory will be applied to the semi-analytical model of § 2. This will provide a semi-analytical description of the parameter regions in which each of the four main types of bifurcation pattern occur. It also allows the existence of the fifth bifurcation diagram, the breaking-wave plus isola pattern, to be determined. The equations (A 1) and (A 2), corresponding to the steady-state, two-term model, have the general form,

$$f_i(b_1, b_2, \beta, b_0, \gamma) = 0, \quad i = 1, 2, \quad (4.1)$$

where β is our choice of bifurcation parameter. The hysteresis bifurcation corresponds to solutions for which a hysteresis loop or fold first occurs in the bifurcation diagram.

This corresponds to the conditions:

$$\frac{d\beta}{db_1} = \frac{d^2\beta}{db_1^2} = 0. \quad (4.2)$$

As the equations (4.1) cannot be rearranged to obtain an explicit relationship for β , the conditions (4.2) are applied by using implicit differentiation. Now, for a given bifurcation diagram γ and b_0 are constant while the first of (4.2) states $d\beta/db_1 = 0$. The total derivative of (4.1) with respect to b_1 is taken, which gives

$$\frac{df_i}{db_1}(b_1, b_2) = f_{ib_1} + f_{ib_2} \frac{db_2}{db_1} = 0, \quad i = 1, 2. \quad (4.3)$$

In (4.3) the f_i are written as functions of b_1 and b_2 . This notation is meant to imply that the f_i depend on b_1 both explicitly and implicitly via b_2 . The second total derivative of (4.1) and the conditions (4.2) gives

$$\frac{d^2f_i}{db_1^2}(b_1, b_2) = 0, \quad i = 1, 2. \quad (4.4)$$

The hysteresis bifurcation points for the two-term model are given by (4.1), (4.3) and (4.4), which represent six equations in the seven variables b_1 , b_2 , β , γ , b_0 , db_2/db_1 and d^2b_2/db_1^2 . Two new variables have been introduced into the system, db_2/db_1 and d^2b_2/db_1^2 , as a consequence of the implicit differentiation. For the one-term model the hysteresis conditions reduce to

$$f = f_{b_1} = f_{b_1 b_1} = 0, \quad (4.5)$$

which represent three equations in the four variables, b_1 , β , γ and b_0 . For both these models the loci of hysteresis points represent a line in the γ – b_0 -plane which, when crossed, causes a hysteresis loop to be created or destroyed in the relevant bifurcation diagram. The sets of transcendental equations for the hysteresis bifurcation points are found using the symbolic manipulation package, REDUCE, and then solved numerically using the root-finding routine from the IMSL library. A similar process is followed in the remainder of the paper to convert the mathematical conditions for the isola bifurcation curve, the isola cusp point and the DZE and transversality Hopf degeneracies into sets of transcendental equations. The isola bifurcation points are defined by

$$\frac{d\beta}{db_1} = \frac{d\gamma}{d\beta} = 0. \quad (4.6)$$

Again, these conditions represent lines in the γ – b_0 -plane which, when crossed, causes an isola to be created or destroyed in the relevant bifurcation diagram.

Figure 5 shows the division of the γ – b_0 -plane into regions corresponding to the different bifurcation diagrams. Shown are the hysteresis and isola curves corresponding to the one-term (solid lines) and two-term (dashed lines) semi-analytical models. Starting in the region with a unique bifurcation pattern and crossing the isola curve causes the birth of an isola at a single point above the low conversion branch. Moving in a clockwise direction on the figure results in the isola curve being crossed for a second time; now the isola merges with the low conversion branch to form a mushroom pattern. When the hysteresis curve is crossed a hysteresis loop is lost

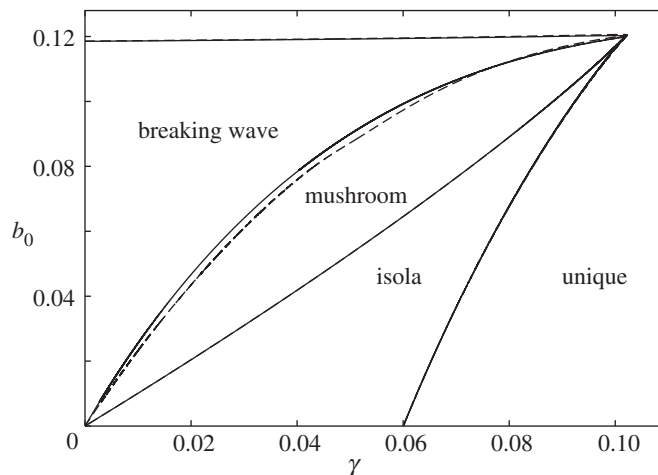


Figure 5. Division of the γ - b_0 -plane into regions corresponding to the different bifurcation diagrams. Shown are the one-term (solid lines) and two-term (dashed lines) semi-analytical curves.

in the mushroom, forming the breaking-wave pattern. The second crossing of the hysteresis curve results in a return to the unique pattern. More details on the transitions between bifurcation diagrams can be found in Kay *et al.* (1987). This figure is qualitatively similar to fig. 6 in Kay & Scott (1988), who obtained their predictions numerically. In fact, a quantitative comparison shows little difference between the two figures at the level of graphical accuracy. For example, the semi-analytical and numerical predictions both show that the intersection of the isola curve with the γ -axis occurs at $\gamma = 0.06$, while the intersection of the hysteresis curve and the b_0 -axis occurs at $b_0 = 0.119$. Also noteworthy is the excellent comparison between the one- and two-term semi-analytical models, indicating the accuracy and usefulness of the simpler one-term model.

The pitchfork bifurcation is a common solution point of the isola and hysteresis conditions, where the isola curve crosses the hysteresis curve, creating a small region of parameter space in which a fifth bifurcation pattern occurs. This scenario occurs in the CSTR reactor for (1.1) with the addition of an uncatalysed conversion step (see Kay *et al.* 1987). If an additional constraint is satisfied, then the most degenerate point is a winged-cusp singularity, and no fifth parameter region occurs, as for (1.1) in the CSTR. The existence of the fifth bifurcation pattern for the semi-analytical model will now be determined, by calculating the locations of the pitchfork bifurcation and the cusp, or turning point, of the isola curve.

The pitchfork bifurcation is given by the combined conditions for the hysteresis and isola bifurcation points, (4.2) and (4.6). The cusp of the isola curve is given by the conditions:

$$\frac{d\gamma}{db_1} = \frac{db_0}{db_1} = 0. \quad (4.7)$$

The equations describing the pitchfork and cusp points are solved numerically to 11 decimal places of accuracy. The pitchfork bifurcation point corresponding to the two-term model is

$$(\gamma, b_0) = (0.102\ 260\ 893\ 90, 0.120\ 519\ 222\ 39).$$

Scott (1987) gives a numerical prediction of the location of the pitchfork bifurcation point as $(\gamma, b_0) = (0.1023, 0.12057)$, hence the semi-analytical prediction is accurate to at least four decimal places. The isola cusp point is given by

$$(\gamma, b_0) = (0.102\,260\,893\,99, 0.120\,519\,222\,57).$$

It can be seen that the pitchfork bifurcation and isola cusp points, while very close together, are not exactly the same. In the γ – b_0 -plane, the two points differ at the tenth decimal place; however, they differ at the fourth decimal place of b_1 . This confirms that the winged-cusp singularity does not occur, as it does for (1.1) in the CSTR. The distance in the γ – b_0 -plane between the pitchfork bifurcation and the isola cusp is 1.7×10^{-10} . Hence an exceedingly small fifth parameter region exists for the two-term semi-analytical model.

Due to the approximate nature of the semi-analytical model, no definite conclusion can be reached on the existence of the fifth parameter region in the full system of partial differential equations. Kay & Scott (1988) could not find this region numerically. If the region does exist, the above results indicate that it is extremely unlikely to be identified either numerically or experimentally.

5. Local stability and oscillatory solutions

Hopf bifurcations and stable oscillatory solutions are known to occur for the system (1.1), both in the CSTR and the reaction–diffusion cell. The theory of Hopf bifurcations can be found in standard texts on bifurcation theory and dynamical systems such as Guckenheimer & Holmes (1983) or Golubitsky & Schaeffer (1985). The local stability of the system (2.1) was considered in Kay & Scott (1988) by calculating the Jacobian matrix of the finite-difference form of the partial differential equations. A region of the γ – b_0 -plane, in which Hopf bifurcations can occur, was identified. Here the stability of the semi-analytical model is considered. The Hopf degeneracy points are calculated to allow a semi-analytical prediction of the region in which Hopf bifurcations occur. This prediction is compared with numerical results.

(a) The one-term model

In this case $a_2 = b_2 = 0$ in (2.3) and the semi-analytical model is described by a pair of ordinary differential equations for a_1 and b_1 . Expanding the two ordinary differential equations about the steady-state solution gives the trace, $\text{tr } J$, and determinant, $\det J$, of the Jacobian matrix $J = (j_{ij})$ as

$$\text{tr } J = j_{11} + j_{22}, \quad \det J = j_{11}j_{22} - j_{12}j_{21}, \quad (5.1)$$

where

$$j_{11} = -\frac{1}{8}\pi^2 + \beta T, \quad j_{12} = \beta S, \quad j_{21} = \beta T, \quad j_{22} = -\frac{1}{8}\pi^2 + \beta S,$$

$$S = -\frac{3}{4}a_1b_1 - \frac{8}{3\pi}(a_1b_0 - b_1) + b_0, \quad T = -\frac{3}{8}b_1^2 - \frac{8}{3\pi}b_1b_0 - \frac{1}{2}b_0^2,$$

and the variables a_1 and b_1 in (5.1) represent steady-state values. The growth of small perturbations is described by the eigenvalues of the Jacobian, which are the solution of the quadratic equation,


$$\lambda^2 - \text{tr } J\lambda + \det J = 0. \quad (5.2)$$

The steady-state solution is stable if both eigenvalues are positive while Hopf bifurcations occur when the eigenvalues are purely imaginary. The conditions for Hopf bifurcations are

$$f = \operatorname{tr} J = 0, \quad \det J > 0, \quad \frac{d \operatorname{tr} J}{d\beta} \neq 0, \quad \mu_2 \neq 0. \quad (5.3)$$

The parameter μ_2 is the leading-order amplitude of the limit-cycle, which can be found using a standard algorithm. Limit-cycles born at the Hopf point can either be stable ($\mu_2 < 0$, a supercritical bifurcation) or unstable ($\mu_2 > 0$, a subcritical bifurcation). To determine the parameter region in which Hopf bifurcations occur, the points for which the bifurcation is degenerate must be found. The degenerate Hopf points are defined by

$$\text{DZE: } f = \operatorname{tr} J = \det J = 0, \quad \text{H2: } f = \operatorname{tr} J = \frac{d \operatorname{tr} J}{d\beta} = 0, \quad (5.4)$$

the double-zero eigenvalue (DZE) enerate points imply that both the eigenvalues are zero, and the transversality (H2) degeneracy occurs when two Hopf points merge on a solution branch with their eigenvalues having a non-zero imaginary part.

(b) *The two-term model*

Now the set of four ordinary differential equations (2.3), which represent the two-term semi-analytical model, are considered. The eigenvalues of the Jacobian matrix are described by the quartic equation,

$$\lambda^4 + \alpha_1 \lambda^3 + \alpha_2 \lambda^2 + \alpha_3 \lambda + \alpha_4 = 0, \quad (5.5)$$

where the coefficients α_i are not presented here but are calculated using the symbolic manipulation package, REDUCE. Hopf bifurcations occur for this system when one pair of eigenvalues are purely imaginary, which implies $q = \alpha_4 \alpha_1^2 + \alpha_3^2 - \alpha_1 \alpha_2 \alpha_3 = 0$. The degenerate Hopf points are given by

$$\text{DZE: } f_1 = f_2 = \alpha_3 = \alpha_4 = 0, \quad \text{H2: } f_1 = f_2 = q = \frac{dq}{d\beta} = 0. \quad (5.6)$$

The loci of the DZE and H2 degenerate Hopf points are lines; when plotted it is found that the DZE curve lies entirely within the H2 curve in the γ - b_0 -plane. This region is qualitatively similar to that for the system (1.1) in the CSTR, see fig. 9 in Gray & Scott (1984). However, for a portion of the H2 degeneracy curve (in the region where $\gamma \rightarrow 0$) the parameter $\beta \rightarrow \infty$. As discussed earlier this is a singular limit in which the diffusive effects become small and the concentration profiles become very flat. In this limit the semi-analytical model breaks down with the concentrations of the autocatalyst and reactant becoming negative. Hence the degeneracy curve represents non-physical solutions in this portion of the plane. This is resolved by considering solutions corresponding to physically realistic Hopf bifurcations only. When the concentration of either the autocatalyst or reactant becomes negative along the H2 degeneracy curves, they are replaced by the conditions,

$$f = \operatorname{tr} J = 1 + a_1 = 0, \quad f_1 = f_2 = q = b_0 + b_1 + b_2 = 0, \quad (5.7)$$

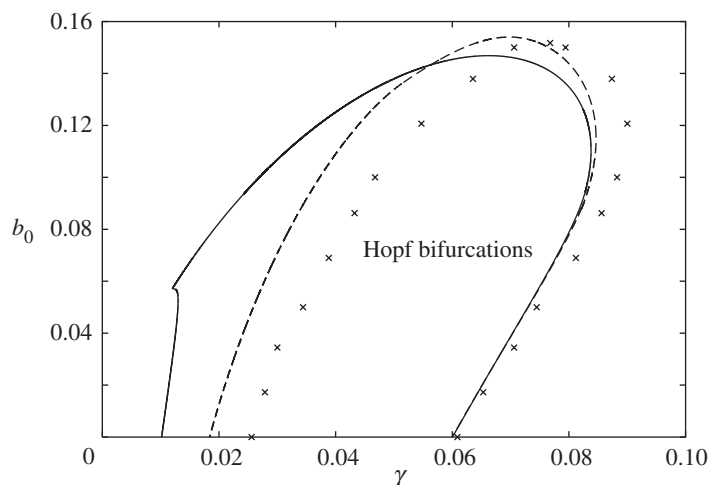


Figure 6. The region of the γ - b_0 -plane in which physically realistic Hopf bifurcations can occur. Shown is the one-term (solid line) and two-term (dashed line) regions and numerical solutions (crosses).

for the one- and two-term models, respectively. These constrain the Hopf points to have non-negative concentrations. The reactant concentration at the reactor centre, $a = 1 + a_1$, is used for the one-term model while the autocatalyst concentration $b = b_0 + b_1 + b_2$ is used for the two-term model simply because these are the relevant quantities which first become negative along their respective H2 degeneracy curves.

Figure 6 shows the region of the γ - b_0 -plane in which physically realistic Hopf bifurcations can occur. Shown is the one-term (solid line) and two-term (dashed line) regions. The crosses are from fig. 6 of Kay & Scott (1988), and represent numerical solutions found using the Jacobian of the discretized version of (2.1). The loci of H2 degeneracy points, given by the second of (5.4) and (5.6), forms the right-hand side of these curves, while on part of the left-hand side the physical degeneracy conditions (5.7) are used. For the two-term solution the H2 curve loses physical validity at the point $(\gamma, b_0) = (0.052, 0.136)$, where $\beta = 532$. It can be seen that the two-term semi-analytical solution is reasonably close to the numerical estimates of Kay & Scott (1988), particularly on the right-hand side of the region. Hence the two-term method gives a good estimate of the parameter region in which Hopf bifurcations can occur.

Figure 7 shows the limit-cycle curve a versus b . The parameters are $\beta = 192.3$, $b_0 = 0.08$ and $\gamma = 0.05$. Shown is the one-term (solid line) and two-term (large dashes) semi-analytical solutions and the numerical solution of (2.1) (small dashes). The numerical solution for this example was also presented in fig. 9 of Kay & Scott (1988) and represents a stable limit-cycle about a steady state on the upper branch of a mushroom bifurcation pattern. On the upper portion (for large a and small b) of the limit-cycle curve the one- and two-term semi-analytical solutions are very accurate, due to the fact this represents a state of low conversion, where the solution is close to the ambient values of $a = 1$ and $b = 0.08$. On the lower-portion of the limit-cycle curve (for small a and large b) there is some divergence between the results. This part of the curve represents a state of high conversion where the autocatalyst concentration is large, and has a non-central maximum. The reactant concentration is small and the profile is very flat near the centre of the reactor. In this case the

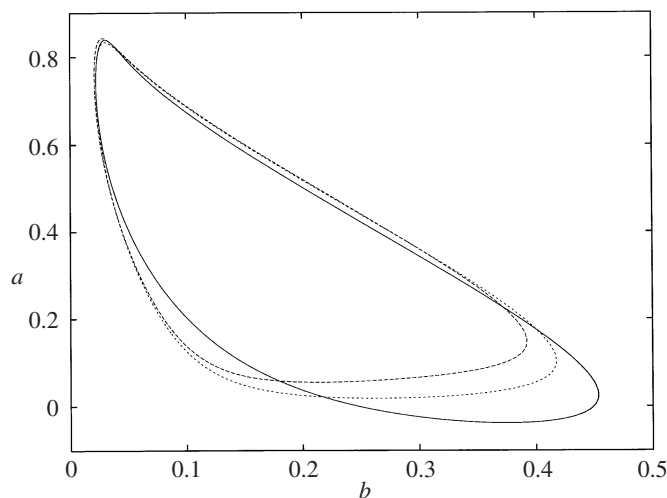


Figure 7. The limit-cycle curve a versus b . The parameters are $\beta = 192.3$, $b_0 = 0.08$ and $\gamma = 0.05$. Shown is the one-term (solid line) and two-term (large dashes) semi-analytical solutions and the numerical solution of (2.1) (small dashes).

one-term solution breaks down, as it predicts a negative reactant concentration, due to its inability to model the flat reactant profile and the non-central autocatalyst peak. The two-term solution, however, remains physical, and is fairly close to the numerical curve. The period of the limit-cycle is found to be 2.40 numerically, while the one- and two-term predictions are 3.31 and 2.46, respectively. The amplitude of the oscillations in the reactant concentration is 0.82, while the one- and two-term semi-analytical predictions are 0.88 and 0.79. The amplitude of the oscillations in the autocatalyst concentration is 0.39, while the one- and two-term predictions are 0.43 and 0.41. Hence, it can be seen that the two-term semi-analytical solution is quite accurate and captures all the essential details of the stable limit-cycle.

6. Conclusion

Semi-analytical solutions have been developed for the cubic-autocatalytic reaction with linear decay in a reaction–diffusion cell. In the semi-analytical model the governing partial differential equations are approximated by ordinary differential equations. Comparisons with numerical solutions show that the two-term semi-analytical model is very accurate. The one-term model is also useful, as it can be obtained explicitly and gives qualitatively correct solutions. The application of singularity theory to the semi-analytical models allows the parameter regions, in which each of the different bifurcation patterns occurs, to be found. Also, in the semi-analytical model, the fifth bifurcation pattern, is found to occur in an extremely small parameter region.

The method used here is a general one, and can be used to develop semi-analytical solutions to other combustion problems involving diffusion. One potential application is a diffusive version of the Sal’nikov thermokinetic oscillator, in which the temperature and concentration are coupled. This reaction involves the two-step decay of a chemical species, where the second step is exothermic and its rate depends on temperature. In this case the Arrhenius law would need to be approximated by a rational-cubic function, using the method of Marchant & Liu (1998).

The author is indebted to the School of Mathematics and Statistics, University College, ADFA, Canberra, Australia, for their hospitality, as some of this work was undertaken during a visit there. The author also thanks Dr G. Mercer and Dr M. Nelson for several useful discussions.

Appendix A. Steady-state equations

The steady-state solution of the two-term model is found as the solution of the two transcendental equations,

$$\begin{aligned}
 f_1 = & -\frac{16}{\pi^3}b_0^3\beta^2\gamma - \frac{4}{\pi^2}b_0^2b_1\beta^2\gamma - \frac{34\,304}{405\pi^4}b_0^2b_1\beta^2\gamma - b_0^2b_1\beta - \frac{512}{35\pi^4}b_0^2b_2\beta^2\gamma \\
 & + \frac{4}{\pi}b_0^2\beta - \frac{896}{27\pi^3}b_0b_1^2\beta^2\gamma - \frac{16}{3\pi}b_0b_1^2\beta - \frac{328}{27\pi^3}b_0b_1b_2\beta^2\gamma - \frac{32}{15\pi}b_0b_1b_2\beta \\
 & + 2b_0b_1\beta - 344\frac{3}{5}\pi^3b_0b_2^2\beta^2\gamma - \frac{144}{35\pi}b_0b_2^2\beta - \frac{4}{\pi}b_0\beta\gamma - \frac{3}{\pi^2}b_1^3\beta^2\gamma - \frac{3}{4}b_1^3\beta \\
 & - \frac{19}{9\pi^2}b_1^2b_2\beta^2\gamma - \frac{3}{4}b_1^2b_2\beta + \frac{8}{3\pi}b_1^2\beta - \frac{22}{9\pi^2}b_1b_2^2\beta^2\gamma - \frac{3}{2}b_1b_2^2\beta \\
 & + \frac{16}{15\pi}b_1b_2\beta - b_1\beta\gamma - \frac{\pi^2}{4}b_1 + \frac{72}{35\pi}b_2^2\beta = 0,
 \end{aligned} \tag{A 1}$$

and

$$\begin{aligned}
 f_2 = & \frac{16}{27\pi^3}b_0^3\beta^2\gamma - \frac{512}{35\pi^4}b_0^2b_1\beta^2\gamma - \frac{4}{9\pi^2}b_0^2b_2\beta^2\gamma - b_0^2b_2\beta - \frac{9\pi^2}{4}b_2 - \frac{3}{4}b_2^3\beta \\
 & - \frac{4}{3\pi}b_0^2\beta - \frac{1076}{135\pi^3}b_0b_1^2\beta^2\gamma - \frac{16}{15\pi}b_0b_1^2\beta - \frac{240}{7\pi^3}b_0b_1b_2\beta^2\gamma - \frac{288}{35\pi}b_0b_1b_2\beta \\
 & + 2b_0b_2\beta + \frac{100}{81\pi^3}b_0b_2^2\beta^2\gamma + \frac{16}{9\pi}b_0b_2^2\beta + \frac{4}{3\pi}b_0\beta\gamma - \frac{1}{\pi^2}b_1^3\beta^2\gamma - \frac{1}{4}b_1^3\beta \\
 & - \frac{38}{9\pi^2}b_1^2b_2\beta^2\gamma - \frac{3}{2}b_1^2b_2\beta + \frac{8}{15\pi}b_1^2\beta + \frac{144}{35\pi}b_1b_2\beta - \frac{1}{3\pi^2}b_2^3\beta^2\gamma \\
 & - \frac{8}{9\pi}b_2^2\beta - b_2\beta\gamma - \frac{568\,832}{8505\pi^4}b_0^2b_2\beta^2\gamma = 0.
 \end{aligned} \tag{A 2}$$

References

- Balakotaiah, V. & Luss, D. 1983 Multiplicity features of reacting systems. *Chem. Engng Sci.* **38**, 1709–1721.
- Golubitsky, M. & Schaeffer, D. G. 1985 *Singularities and groups in bifurcation theory*. Springer.
- Gray, P. 1988 Instabilities and oscillations in chemical reactions in closed and open systems. *Proc. R. Soc. Lond. A* **415**, 1–34.
- Gray, P. & Scott, S. K. 1983 Autocatalytic reactions in the isothermal continuous, stirred tank reactor: isolas and other forms of multistability. *Chem. Engng Sci.* **38**, 29–43.
- Gray, P. & Scott, S. K. 1984 Autocatalytic reactions in the isothermal continuous, stirred tank reactor: oscillations and instabilities in the system $a + 2b \rightarrow 3b$; $b \rightarrow c$. *Chem. Engng Sci.* **39**, 1087–1097.
- Gray, P. & Scott, S. K. 1990 *Chemical oscillations and instabilities: nonlinear chemical kinetics*. Oxford University Press.
- Guckenheimer, J. & Holmes, P. 1983 *Nonlinear oscillations, dynamical systems, and bifurcations of vector fields*. Springer.

- Kay, S. R. & Scott, S. K. 1988 Multiple stationary states, sustained oscillations and transient behavior in autocatalytic reaction–diffusion equations. *Proc. R. Soc. Lond. A* **418**, 345–364.
- Kay, S. R., Scott, S. K. & Lignola, P. G. 1987 The application of singularity theory to isothermal autocatalytic reactions: the influence of uncatalysed reactions. *Proc. R. Soc. Lond. A* **409**, 433–448.
- Liu, B. & Marchant, T. R. 1999 The microwave heating of two-dimensional slabs with small Arrhenius absorptivity. *IMA J. Appl. Math.* **62**, 137–166.
- Marchant, T. R. & Liu, B. 1998 The steady-state microwave heating of slabs with small Arrhenius absorptivity. *J. Engng Math.* **33**, 219–236.
- Scott, S. K. 1987 Isolas, mushrooms and oscillations in isothermal, autocatalytic reaction–diffusion equations. *Chem. Engng Sci.* **42**, 307–315.